Radar-based Studies of Mesoscale Convective Storms Using Different Frequency Bands of Weather Radars

CHAN Ying-wa, JIN Jeffrey Tong

Hong Kong Observatory, Hong Kong, China

Abstract

Integrated radar-instrument analyses were conducted for a number of mesoscale convective storms (MCS) that affected Hong Kong in 2021-2022 using different frequency bands of weather radars, wind profiler as well as anemometer, lightning and weather camera networks operated by the Hong Kong Observatory (HKO). The radars included two S-band (3 GHz) weather radars at Tai Mo Shan (TMS) and Tate's Cairn (TC) respectively, a C-band (5 GHz) Terminal Doppler Weather Radar (TDWR) at Brothers Point (BP) and an X-band (10 GHz) Phased Array Weather Radar (PAWR) at Sha Lo Wan (SLW). The S-band radar at TC and the PAWR were dual-polarisation weather radars.

Three different MCS cases causing high impact weather in Hong Kong including hail, waterspout, microburst and windshear that occurred chronologically on 16 September 2021, 8 June 2022 and 18 September 2022 respectively have been examined. For the 1st case, the PAWR enabled detailed observations of the structures of convective cells with hails detected at an altitude range of 3 to 7 km and the 0°C freezing height was estimated to be around 4 km. Hail stones fell on the ground with sizes of around 1 cm or less were reported by members of the public. The presence of mixed ice crystals and graupels promoted cloud electrification, resulting in active cloud-to-cloud and cloud-to-ground lightnings. Hails could also be identified from the hydro-classification products from the S-band weather radar at TC but it was difficult to analyse the detailed structures of the convective cells.

For the 2nd case, the waterspout whose lifetime was less than half an hour was well captured by HKO's weather camera and the PAWR. The horizontal extent and vertical height of the associated velocity couplet observed by the PAWR were over 1 km and 5 km respectively while the maximum velocity was estimated to be above 16 m/s. In this case, signals from the two S-band radars showing the potential formation of a vortex tube associated with the waterspout were not as strong as the PAWR.

The 3rd case was related to thundery showers triggered by intense insolation and it caused the development of microburst and significant windshear as detected by the BP TDWR. During the impact of microburst, the BP TDWR once outputted shear magnitude of over 36 m/s although the sign of an upper-level mesocyclone was not apparent. The differential reflectivity (Z_{DR}) from the PAWR was a good indicator for diagnosing vertical motion with positive and negative Z_{DR} indicating updraughts and downdraughts respectively. In connection to the microburst-producing downdraught, the PAWR showed negative Z_{DR} column in the height range of 0.5 to 4 km. Based on the cross-sections of PAWR images, a region of high winds was observed to descend downwards from about 2 km to the surface in less than 20 minutes and the touch down caused strengthening of surface winds to strong force level as well as around 5°C drop of air temperatures as recorded by one of the HKO's automatic weather stations. Coincidentally, the wind profiler showed a vertical downward velocity of about 8 m/s at a height range of 0.9–1.4 km. Regarding the maximum radar reflectivity of the intense echo triggering the microburst, by comparing the respective low-level PPI images, the two S-band radars showed similar level of around 55 dBZ. It was 1-2 dBZ lower for the C-band BP TDWR which was reasonable as there was no correction of attenuation caused by precipitation. For the X-band PAWR, it was 4-5 dBZ higher which suggested that the associated attenuation correction was overdone.

In summary, a comparison of the different frequency bands of weather radars suggested that the PAWR was more able to capture the mesoscale features of convective cells such as waterspout due to high spatial resolution (30 m) of the PAWR imagery. Also, the PAWR could depict more clearly different hydrometeors, for examples, hails, ice crystals and graupels embedded within convective cells. While the BP TDWR detected the occurrence of microburst and determined the severity of windshear to support HKO's aviation weather services for the operation of the Hong Kong International Airport (HKIA), the complementary use of dual-polarisation PAWR enabled a better appreciation of the positions and strength of updrafts and downdraughts through the use of Z_{DR} columns and using S-band radars to better assess the intensity of radar echoes. Coupled with other instruments' observations, a more thorough understanding on the evolution of MCS was achieved.

Weather Radars and Automatic Weather Stations Network

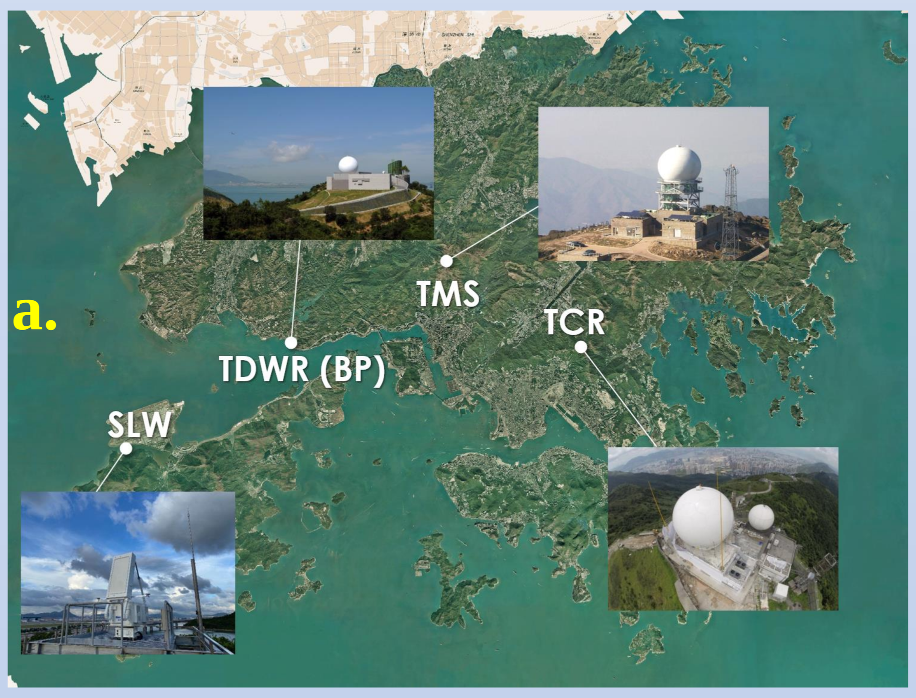

Fig. 1: Observation networks of (a) Weather Radars and (b) Automatic Weather Stations.

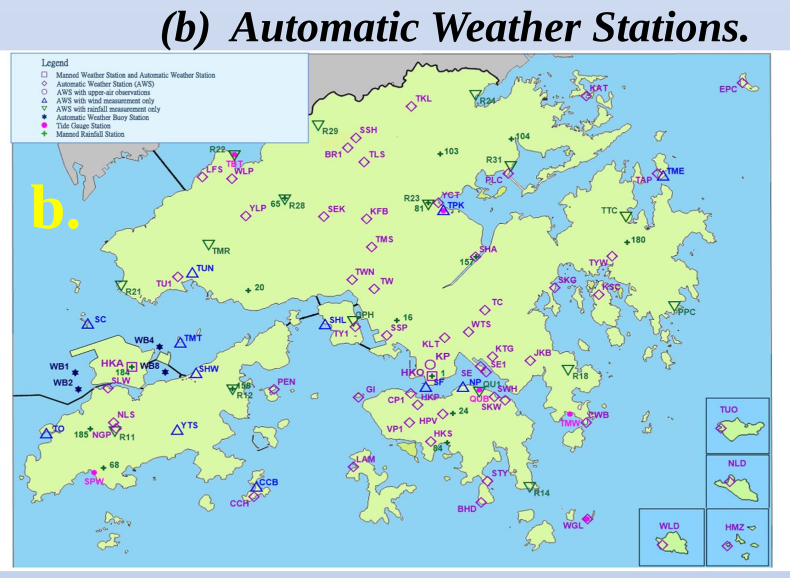

Table 1: Different frequency bands of weather radars used for studying Mesoscale Convective Storms (MCS).

Parameter	TMS	TCR	BP TDWR	SLW PAWR
Height of Antenna (AMSL)	~ 968m	~ 583m	~ 80m	~ 35 m
Polarization	Single	Dual	Single	Dual
Antenna Diameter	8.5m	8.5m	7.9m	~ 1 m x 0.5 m
Antenna Beam Width	0.9°	≤ 1.0°	0.55°	≤ 3.6° (Azimuth) ≤ 1.8° (Elevation)
Transmitter	Klystron	Klystron	Klystron	Solid-state
Transmitter Frequency	2.82 GHz (S-band)	2.92 GHz (S-band)	5.625 GHz (C-band)	9.608 GHz (X-band)
Maximum Range	512 km (Reflectivity) 256 km (Doppler)	512 km (Reflectivity) 256 km (Doppler)	≥ 90 km	60 km
Horizontal resolution	~ 150m	~ 150m	~ 150m	~ 30m
Nyquist velocity	~ 46 m/s	~ 45 m/s	≥ 60 m/s	~ 24 m/s

Case 1: Hails (small hailstones with sizes of < 1cm were reported)

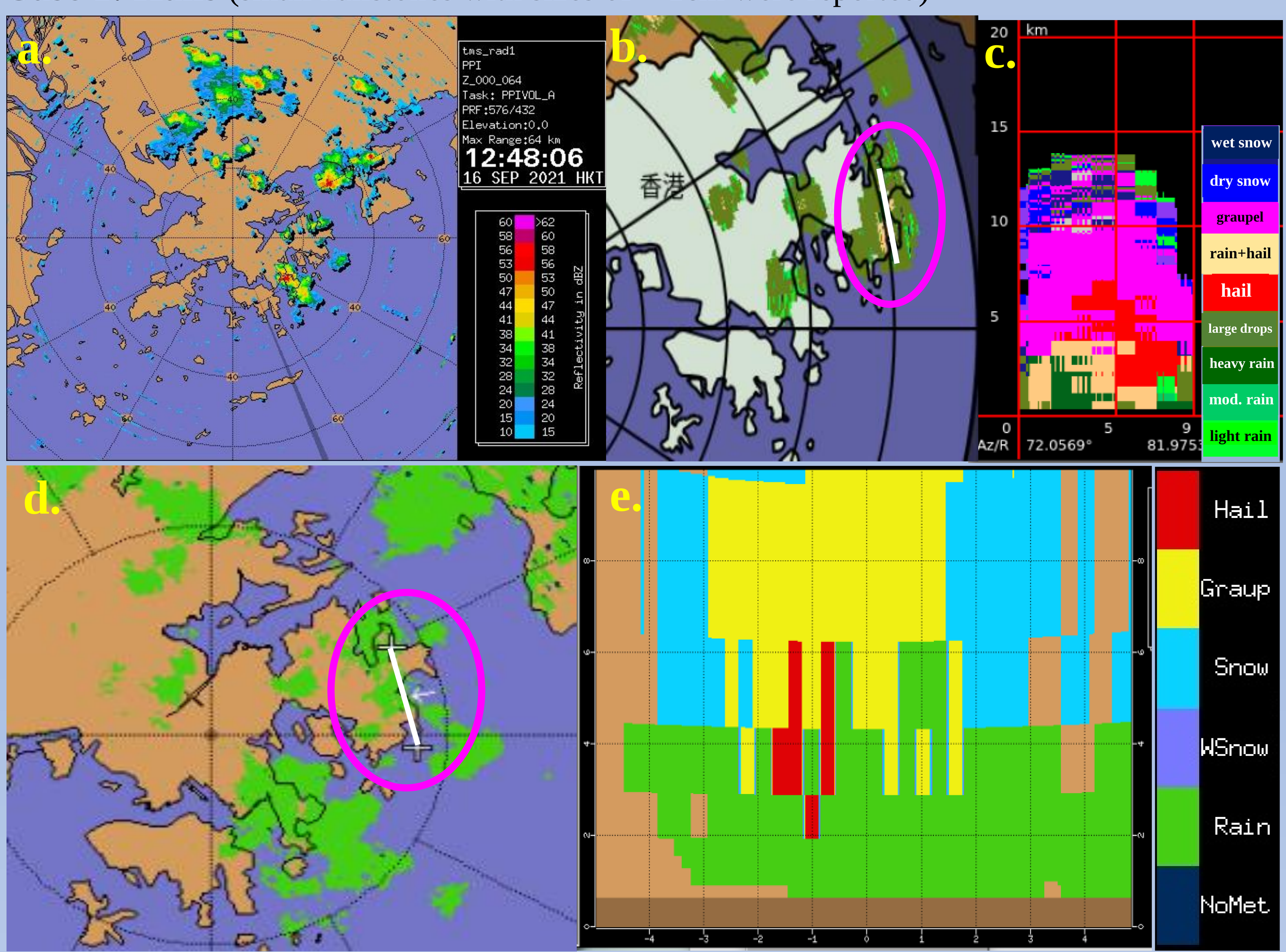

Fig. 2: (a) TMS 0.0° PPI radar reflectivity images at around 12:48 Hong Kong Time (HKT) on 16 September 2021; (b) Hydro-classification product (HCL) from SLW PAWR at 12:55 HKT on the same day with purple circle indicating area of strong convection with signs of hail and white line showing where the cross-section in (c) was made; (c) Cross-section of HCL made along the white line in (b); (d) same as (b) but for HCL from TCR and (e) Cross-section of HCL made along the white line in (d). SLW PAWR detected mixture of hails and rain near the surface while TCR detected hails at height of greater than 2km above the surface.

Case 2: Waterspout

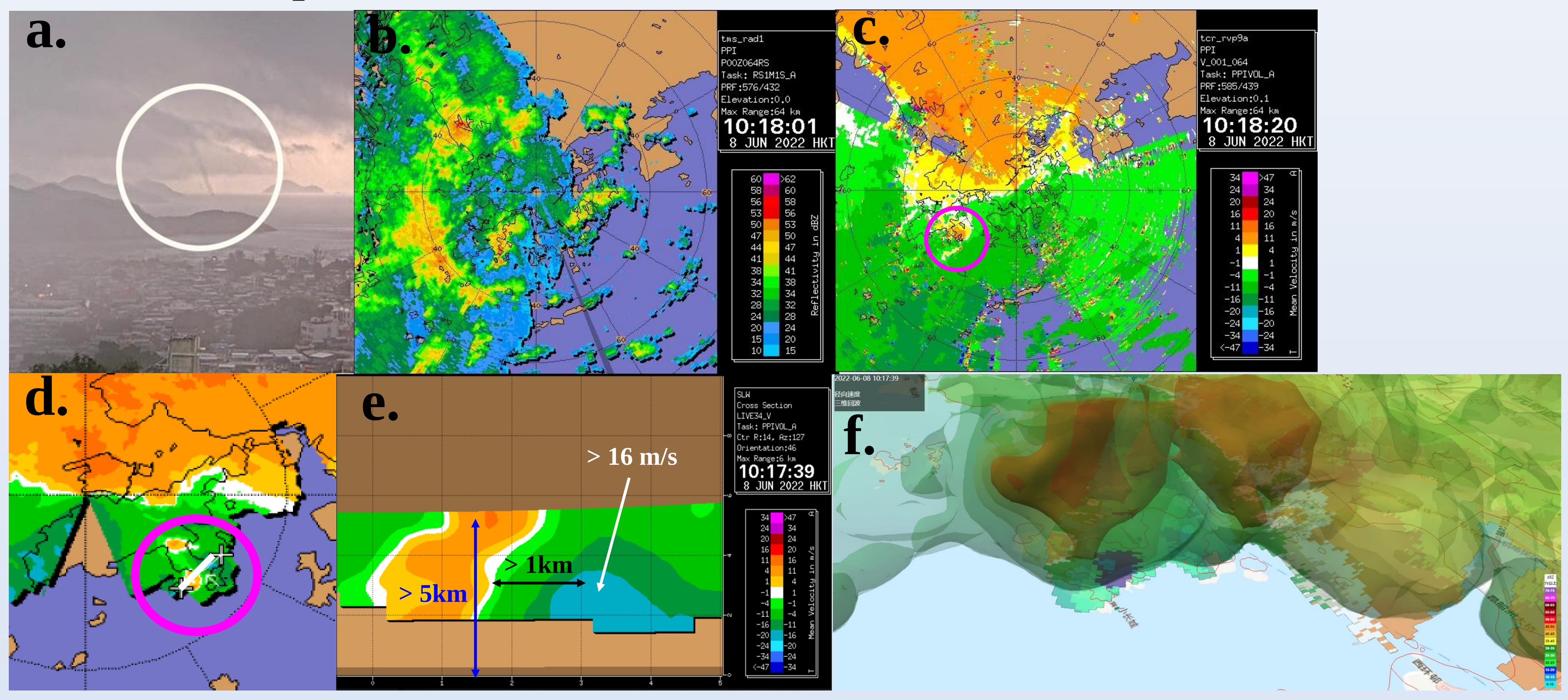

Fig. 3: (a) Waterspout observed by HKO's weather camera at Cheung Chau in the morning of 8 June 2022; (b) and (c) TMS 0.0° PPI reflectivity and TC 0.0˚PPI Doppler velocity images at ~10:17 HKT on that day respectively; (d) Doppler velocity (V) image from SLW PAWR with purple circle indicating the signal of a waterspout and the white line showing where the cross-section in (e) was made; (e) Cross-section of V made along the white line in (d); (f) 3-D image from the SLW PAWR showing the Dual Doppler velocity couplet and the sign of a vortex tube near the centre of the couplet.

Case 3: Microbursts near HKIA (Z_{DR} trough => downdraughts)

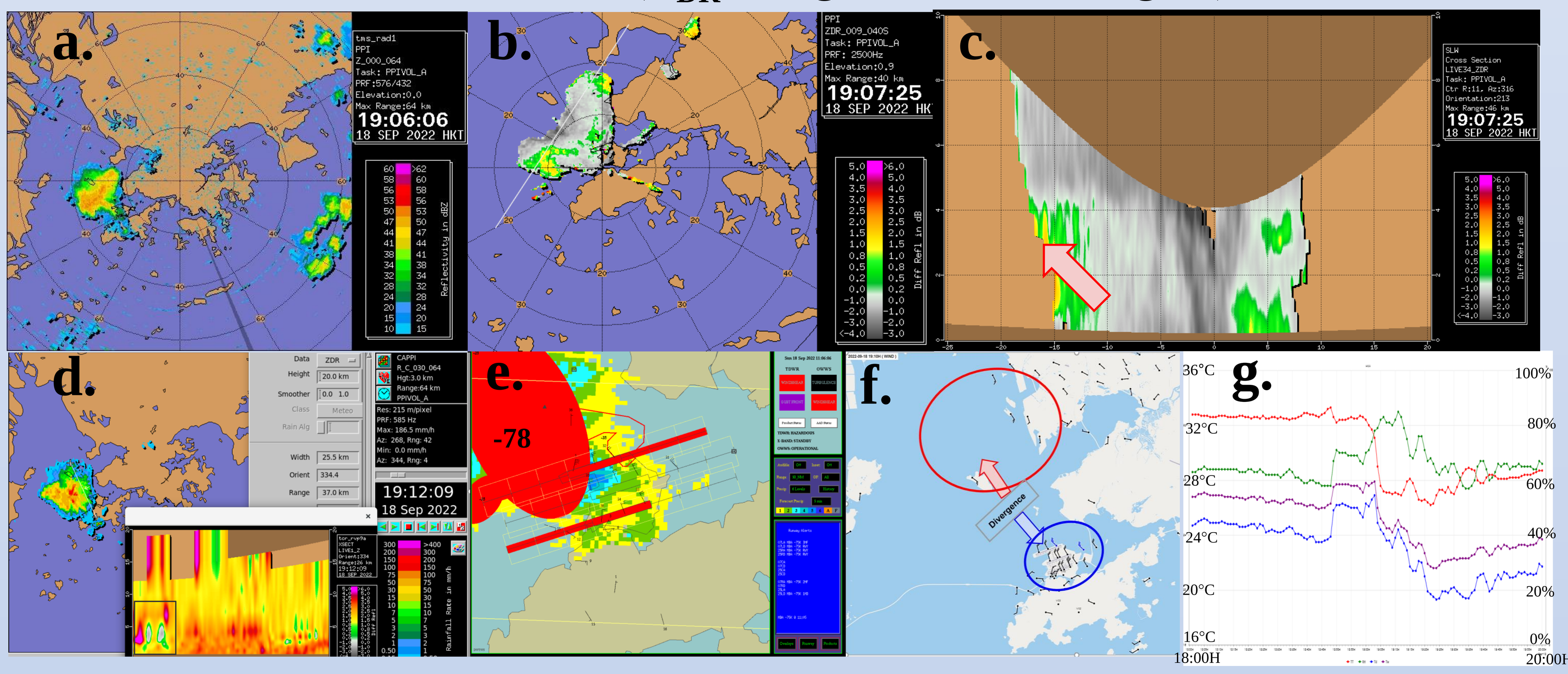

Fig. 4: (a) TMS 0.0° PPI radar reflectivity images at ~19:06 HKT on 18 September 2022; (b) Cross-section of differential reflectivity (Z_{DR}) from SLW PAWR at 19:07 HKT on the same day with white line showing where the cross-section in (c) was made; (c) Cross-section of Z_{DR} made along the white line in (b) showing Z_{DR} trough; (d) Z_{DR} trough also observed from cross-section of TCR at ~19:12 HKT; (e) Windshear alert issued by BP TDWR at ~19:06 HKT; (f) Surface winds at ~19:10 HKT showing area of divergence to the northwest of HKIA; (g) Time series of air temperature (red), wet-bulb temperature (purple), dew point temperature (blue) and relative humidity (green) from 18:00 to 20:00 HKT on that day showing significant drop of temperatures due to the downdraughts.

Case 4: Cloud Electrification (Negative K_{DP} => vertically aligned ice crystals)

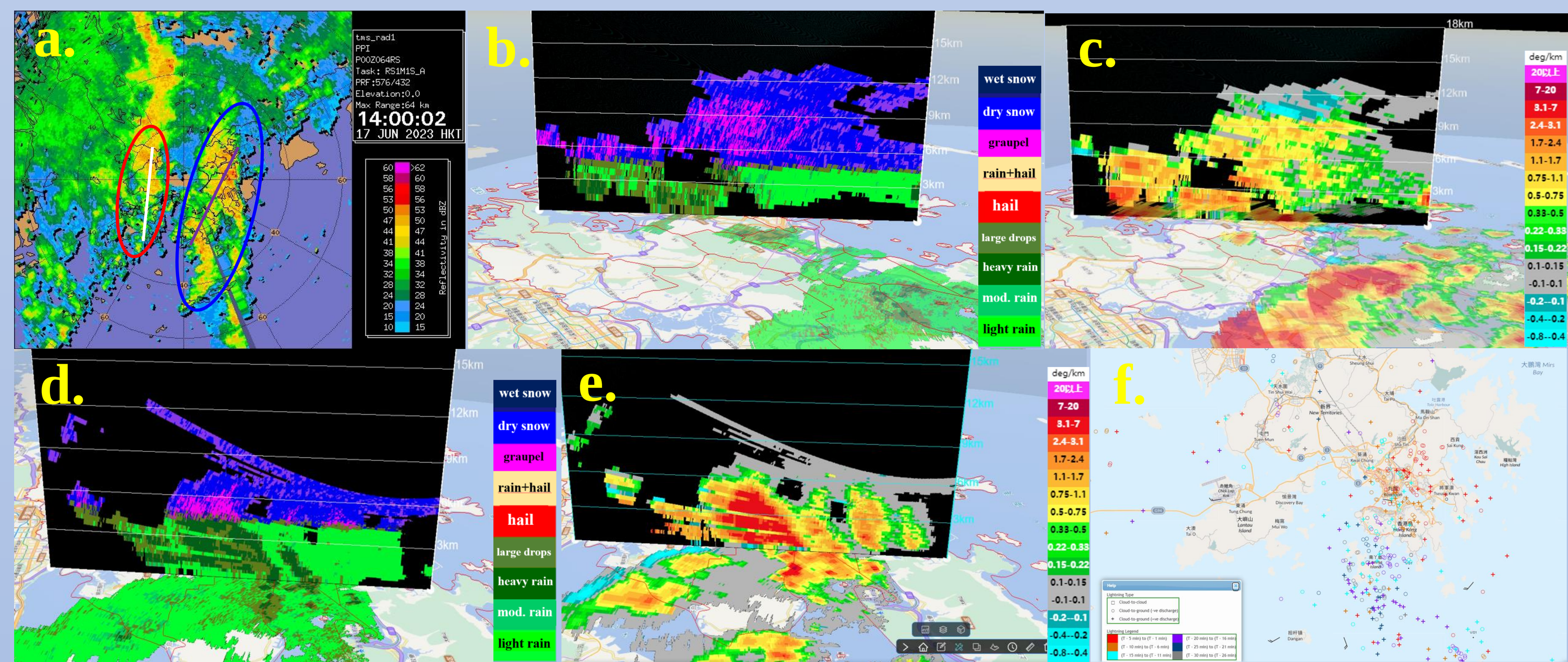

Fig. 5: (a) TMS 0.0° PPI radar reflectivity images at ~14:00 HKT on 17 June 2023; (b) Cross-section of HCL from SLW PAWR along the purple line in (a) showing the separation of rain (green) and snow (blue) and graupel (pink), suggesting the presence of 0°C line; (c) Cross-section of specific differential phase (K_{DP}) along the purple line showing negative K_{DP} for height above 9 km, suggesting the presence of vertically aligned ice crystals; (d) Cross-section of HCL from SLW PAWR made along the white line in (a); (e) Cross-section of K_{DP} showing positive K_{DP} for below 6 km, suggesting mostly rain contents; (f) Distribution of cloud-to-ground lightning.

Summary and Conclusion

The two S-band radars at TMS and TC respectively were good in measuring the reflectivity of the MCSs while the C-band TDWR enabled detection of the severity of windshear and microburst. In comparison, the SLW PAWR captured well the MCSs' structures due to high spatial resolution (30m). Different hydrometeors embedded in the MCSs including rain, hail, ice crystal and graupel can be clearly shown to enable identification of the 0°C temperature line and analysis of the dual-polarisation parameters, e.g. negative Z_{DR} which might be related to downdraughts and negative K_{DP} suggesting the presence of vertically aligned ice crystals.

References

Jin, J. and Y.W. Chan, 2023: Application of the Phased Array Weather Radar at Sha Lo Wan in monitoring high impact weather in Hong Kong, 35th Guangdong-Hong Kong-Macau Seminar on Meteorological Science and Technology, Hong Kong, 20-21 February 2023.

Kuster, C.M., P.L. Heinselman and T.J. Schuur, 2016: Rapid-Update Radar Observations of Downbursts Occurring within an Intense Multicell Thunderstorm on 14 June 2011, *Wea. Forecasting*, **31**, 827-851, doi:10.1175/WAF-D-15-0081.1.

Mattos, E.V., L.A.T. Machado, E.R. Williams, and R.I. Albrecht, 2016: Polarimetric radar characteristics of storms with and without lightning activity, *J. Geophys. Res. Atmos.*, **121**, 14, 201-14, 220, doi:10.1002/2016JD025142.